Enhanced EV charging algorithm considering data-driven workplace chargers categorization with multiple vehicle types

eTransportation 20 (2024) 100326

Contents lists available at ScienceDirect

eTransportation

journal homepage: www.journals.elsevier.com/etransportation

Enhanced EV charging algorithm considering data-driven workplace chargers categorization with multiple vehicle types

Cesar Diaz-Londono [a], Gabriele Fambri [b], Paolo Maffezzoni [a], Giambattista Gruosso [a,*]

[a] Dipartimento di Elettronica, Informazione e Bioingegneria, Politecnico di Milano, Piazza Leonardo Da Vinci, 32, Milan, 20133, Italy
[b] Dipartimento Energia, Politecnico di Torino, Corso Duca degli Abruzzi, 24, Torino, 10129, Italy

ARTICLE INFO

Keywords:
Electric vehicle charger
Non-ideal battery
Flexibility
Model predictive control
Smart charger

ABSTRACT

The increasing penetration of Electric Vehicles (EVs) presents significant challenges in integrating EV chargers. To address this, precise smart EV charging strategies are imperative to prevent a surge in peak power demand and ensure seamless charger integration. In this article, a smart EV charging pool algorithm employing optimal control is proposed. The main objective is to minimize the charge point operator's cost while maximizing its EV chargers' flexibility. The algorithm adeptly manages the charger pilot signal standard and accommodates the non-ideal behavior of EV batteries across various vehicle types. It ensures the fulfillment of vehicle owners' preferences regarding the departure state of charge. Additionally, we develop a data-driven characterization of EV workplace chargers, considering power levels and estimated battery capacities. A novel methodology for computing the EV battery's arrival state of charge is also introduced. The efficacy of the EV charging algorithm is evaluated through multiple simulation campaigns, ranging from individual charger responses to comprehensive charging pool analyses. Simulation results are compared with those of a typical minimum-time strategy, revealing cost reductions and significant power savings based on the flexibility of EV chargers. This novel algorithm emerges as a valuable tool for accurately managing the power demanded by an EV charging station, offering flexible services to the electrical grid.

1. Introduction

In recent years, the proliferation of Electric Vehicles (EVs) on roads signifies a rapid growth in EV penetration. To support this expansion, 22 million charging points need to be added annually [1]. Currently, a substantial number of EV charging events occur in residential and workplace locations, posing significant challenges to charging performance. Consequently, there is a pressing need to develop smart algorithms capable of effectively managing residential and workplace EV chargers. These strategies must prevent an increase in peak demand and offer flexibility to the electrical grid [2].

In the existing literature, numerous studies leverage published EV data sources to validate charging strategies. However, these datasets often suffer from limited information, necessitating assumptions for parameter estimation [3]. Various efforts have been made to classify and assess multiple EV databases, shedding light on EV owners' behaviors and their favored connection points [4]. Studies have categorized EV charging sessions based on both systematic and non-systematic patterns of owners' behavior [5]. The classification of connection points encompasses domestic [6], public, shopping centers, workplaces [7], and commercial for EV fleets [8]. While a preference for workplace charging is notable, particularly among EV owners residing far from their workplace [9], it is noteworthy that a comprehensive categorization of workplace charger behaviors is markedly absent in the existing literature. In addition to location-based classification, charging sessions are further categorized based on their duration [10]. These datasets have been instrumental in various research endeavors. For example, a data-driven framework aimed at assessing the quality of experience for each EV charger is formulated in [11], utilizing metrics to understand the utilization of charging infrastructure in the public sector. Another data is employed to conduct a thorough assessment of energy use patterns and charging load profiles for light-duty EV fleets in Beijing [12]. Despite the evident importance and impact of EV workplace chargers, it is striking that a specific categorization of this sector, outlining the various charger behaviors, is noticeably lacking in the current literature.

In the realm of EV charging strategies, scholars emphasize the importance of implementing smart charging algorithms to mitigate the impact on peak demand. These algorithms, classified as centralized, decentralized, and hierarchical control architectures [13], contribute to reducing operating costs for EV Charge Point Operators (CPOs) by

* Corresponding author.
E-mail address: giambattista.gruosso@polimi.it (G. Gruosso).

https://doi.org/10.1016/j.etran.2024.100326
Received 11 February 2023; Received in revised form 7 March 2024; Accepted 11 March 2024
Available online 15 March 2024

optimizing consumption periods. The work presented in [14] showcases the reduction of operational costs in microgrids through the optimization of electric power dispatch for EVs. Minimizing the cost for EV owners is achieved by forecasting the energy required for the next trip [15], as explored in the relevant literature. In [16], the evaluation of benefits and remuneration levels for EV users in the context of smart charging strategies is discussed. Smart charging strategies for EV car-sharing, grounded in real data, not only effectively manage EV fleets but also integrate renewable sources and electrical loads [17]. Additionally, multi-objective strategies, exemplified by the work in [8], aim to maximize revenues from providing energy services while minimizing the cost associated with parking. The methodology presented in [18] focuses on minimizing the total annual scheduling costs for multiple vehicle types in public transport. Real-time simulators, as evidenced by [19], are instrumental in testing Energy Management Systems (EMS) in microgrids, thereby minimizing costs for both EV owners and workplace chargers. Other sophisticated approaches, like state–space methods for frequency regulation [20] or Model Predictive Control (MPC) for reducing losses in the grid and enhancing the comfort of EV users [21], have been explored. In [22], the evaluation of the welfare maximization-based soft actor–critic model to mitigate transformer overload in distribution systems due to the high penetration of EVs is presented. However, a common limitation among most existing algorithms is the oversight of crucial implementation features, such as actual EV Supply Equipment (EVSE) output levels and non-ideal EV battery responses. This gap highlights the need for charging algorithms that comprehensively consider these practical aspects for more effective and accurate results.

A pivotal factor for EV smart algorithms lies in the flexibility capacity that an EV charger can offer to the electrical grid. In [23], EV charger flexibility is defined based on nominal EV battery charging profiles. This flexibility can be measured in terms of connection duration and energy [24] or solely in time duration, representing the difference between the time the EV is connected and the time it needs for charging [25]. Workplace chargers' dynamic flexibility is delineated in [26], considering the actual upward and downward flexibility an EV can provide to the system operator at any connection time. Recent research delves into how plug-in behaviors influence flexibility capacity [27]. Moreover, due to its flexibility, EVs can participate in ancillary services [28]. In [29], a compensation mechanism enabling EV users to receive compensation for flexibility services is presented. However, none of these studies consider both the charging profiles of individual EV batteries and the evaluation of flexibility across different categories of workplace EVSE.

This article addresses critical gaps in the literature by aiming to comprehensively cover: (i) a specific categorization of EV workplace charger behavior; (ii) identification of non-ideal EV battery profiles; (iii) a smart charging algorithm that considers actual implementation features, such as EVSE output levels and non-ideal EV battery response; (iv) evaluation of flexibility in different categories of workplace chargers. Consequently, we propose an EV charging algorithm for an EV CPO based on optimal control, incorporating a cost-minimization and maximum flexibility strategy [23]. While some research evaluates non-ideal EV battery behavior, considering factors like preprocessing datasets and training regression models [30], or reviewing battery thermal management systems [31], the integration of these findings into smart charging strategies is often overlooked. Our enhanced algorithm considers actual EVSE pilot signal standards and non-ideal EV battery responses, estimated through a data-driven process. Operating on Model Predictive Control (MPC), the algorithm manages multiple vehicle types, accommodating diverse EV battery capacities and rated powers. Inputs include arrival and departure times, arrival State-of-Charge (SoC), and requested energy for each EV. We also develop a data-driven categorization for workplace chargers based on historical energy delivery data, contributing to the understanding of workplace charger behavior. Additionally, EV arrival SoCs are not reported in the charging sessions; in the literature, some approaches have been followed to suggest the arrival of SoCs. In [32], the arrival SoC is set to be 50% for all EVs; in [33], the arrival SoC is assumed to be sent by an EV app to the charging station operator; while in [34] the arrival SoC is taken between 40% and 55%. We propose a new data-driven straightforward methodology for estimating EV arrival SoC distributions. The paper concludes with an analysis of workplace chargers' flexibility, considering idle periods, power levels, and different arrival SoCs, showcasing higher flexibility capacities with higher arrival SoCs.

In summary, the main contributions of this article are:

- *Enhanced EV Smart Charging Algorithm*: Introducing an optimized algorithm for EV smart charging that accounts for non-ideal EV battery responses, accommodates multiple vehicle types, and adheres to the EVSE pilot signal standard.
- *Non-ideal EV Battery Response Estimation*: Employing data-driven processes for the accurate estimation of non-ideal EV battery responses.
- *Workplace EV Charger Categorization*: Utilizing a data-driven strategy to categorize workplace EV chargers, providing a systematic framework for understanding their diverse behaviors.
- *Methodology for Arrival SoC Distributions*: Proposing a novel methodology for estimating the distributions of arrival State-of-Charge (SoC) for workplace chargers, including the distributions of arrival and departure times.
- *Analysis of EV Charger Flexibility and Maximum Power Reduction*: Conducting a comprehensive analysis of the flexibility exhibited by EV chargers, coupled with the computation of maximum power reduction for identified workplace charger categories.

The subsequent sections detail the challenges faced by an EV CPO, the non-ideal EV battery estimation, and workplace data-driven characterization (Section 2). Section 3 thoroughly describes our enhanced EV charging algorithm, and Section 4 presents and compares the results with a standard strategy. Finally, Section 5 discusses the conclusions and outlines avenues for future work.

2. Challenges and data-driven processes of an EV CPO

This section outlines the challenges encountered by an Electric Vehicle (EV) charging algorithm operated by a workplace Charger Point Operator (CPO). Subsequently, it delves into the identification of actual EV battery charging profiles derived from real-world data. The analysis covers various arrival and departure times, along with the energies delivered. Leveraging this energy data, we formulate a strategy to determine the State of Charge (SoC) of the EVs upon arrival. The resulting EV battery profiles, connection times, energies, and arrival SoCs collectively serve as inputs for the CPO charging algorithm.

2.1. CPO challenges

The challenge faced by the CPO lies in effectively overseeing the entire charging pool, encompassing all Electric Vehicle Supply Equipments (EVSEs), i.e., all its chargers. This involves defining distinct charging profiles for each EV while accommodating EV owner preferences, optimizing operational costs, and mitigating peak power demands.

As illustrated in Fig. 1, the schematic diagram depicts the various elements within the charging pool that are managed by the CPO, including different types of EVs. These EVs may possess varying battery capacities and distinct input power specifications. Furthermore, the actual charging profiles of EV batteries are non-ideal, exhibiting variations over time based on the EVSE pilot signal and the power accepted by the EV Battery Management System (BMS). Consequently, the charging algorithm must be capable of effectively handling diverse EV types equipped with non-ideal batteries and considering different EV arrival SoC distributions.

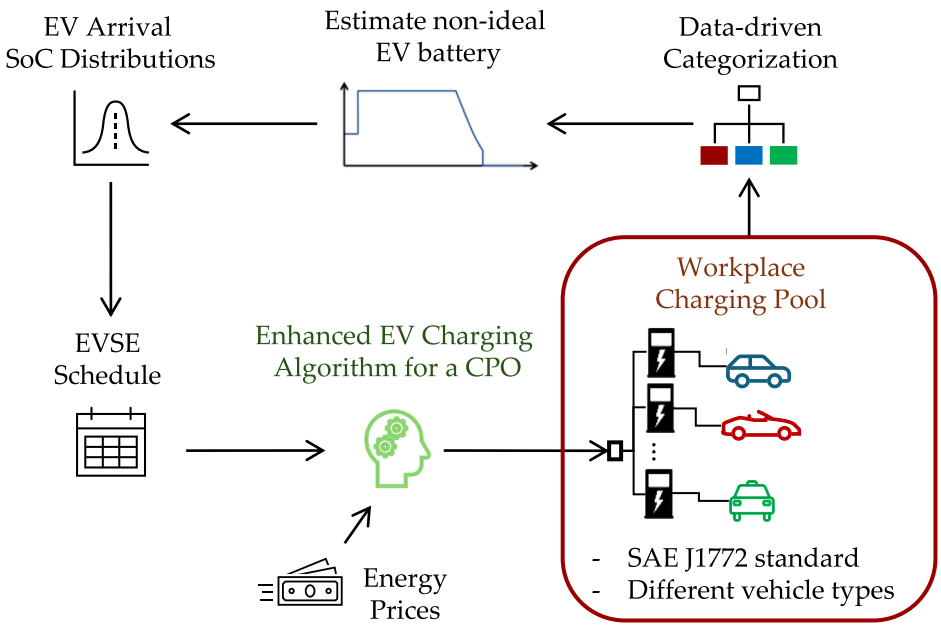

Fig. 1. General scheme for a workplace changing pool managed by a CPO. The EV charging algorithm operates the pool, taking into account charger scheduling, energy prices, and the real-time responses of both vehicles and chargers (EVSE).

Furthermore, the majority of commercial EVSEs only support a discrete set of pilot signals. For instance, one of the common standards used in the United States is the SAE J1772 [35]. According to this standard, when an EV is charging, the minimum pilot current is 6 A, and the maximum is 80 A, with discrete control operating in steps of 1 A.

The EV CPO should have the capability to reduce its operating costs and receive incentives for providing flexibility services or reducing peak power. These profits are maximized by understanding the features of EV users and their charging behaviors, leading to a more effective schedule concerning energy prices.

2.2. Data-driven methodology

In this subsection, we propose the methodology employed by the CPO to address its challenges. This involves identifying actual EV charging profiles based on real-world data, calculating diverse arrival and departure times, and delivered energies, as well as estimating the arrival SoC of EVs. These inputs are crucial for feeding the optimal charging algorithm.

The methodology considers six phases, as illustrated in Fig. 2. It initiates with data preparation, focusing on clean data. Subsequently, various charging profiles are identified, considering non-ideal battery model parameters. Following this, a data-driven process is executed to classify workplace chargers based on the identified charging types, providing distributions of EV behaviors. The selected category or categories for evaluation are then computed and the arrival SoC distributions are estimated. Finally, utilizing these distributions and the non-ideal battery parameters, the schedule for the chargers is formulated to feed the optimal algorithm. The algorithm receives the scenario information and is subsequently executed, with its solution compared to a benchmark strategy. In the following subsections, each phase of the methodology is outlined.

2.2.1. Data preparation

The EV charging dataset ACN-Data [36] is analyzed, specifically focusing on the Caltech site (California Institute of Technology, Pasadena, CA, USA). This site encompasses 55 EVSEs and provides data spanning from April 25, 2018, to September 14, 2021. The dataset reports vital information such as user ID, obtained through a Mobile App; station ID, corresponding to the EVSE ID; connection time; done charging time; disconnection time; energy delivered; and energy requested, among other details. the time series of the charging events are documented with a non-constant sample time of approximately 4 s.

To delineate typical EV user charging profiles, a pre-processing analysis is conducted. The data horizon considered excludes the period of strict lockdown during the pandemic due to the negligible EV usage. Therefore, data from February 1, 2020, to November 18, 2020 (the first data reported after the pandemic) are not taken into account. In this evaluated period, 15,249 charging events from 555 users are reported.

2.2.2. Non-ideal EV battery estimation

The EVSEs in the database adhere to the Society of Automotive Engineers standard SAE J1772 for level 2 charging. Consequently, by considering not only the current time-series but also the current limits specified in the standard, the database is categorized into three distinct types of charging profiles. Upon analyzing the current time-series and recognizing three maximum currents reported (32 A, 16 A, and 10 A), we delineate the database into three charging profile types, distinguished by the maximum current consumption of the EVs (see Fig. 3).

Fig. 4 provides an illustrative example profile for each type. The gray areas depict the duration of the EV connection, while the blue profiles showcase the actual EV current profiles.

The three identified charging types adhere to the EV battery charging profile depicted in Fig. 5, which encompasses three stages. Firstly, a Pre-Charge (PC) current I_{pre} is applied after the EV's connection and lasts for Δ_1. Subsequently, Maximum Current (MC) I_{chg} and Charging Tail (CT) stages are executed, operating for durations Δ_2 and Δ_3, respectively. At the end of the CT stage, the current arrives at I_{end} before dropping to zero current. However, it is observed that not all stages are present in all EV charging profiles in the actual data.

Table 1 presents the estimated EV battery charging parameters, maximum energy, and power injected into the EVs for each type. The typical current levels at each stage, i.e., the mean currents of I_{pre}, I_{chg}, and I_{end}, are computed. Most I_{pre} values are zero (not considered for the values in the table), indicating that charging events typically commence in the MC stage. Therefore, time Δ_1 is zero for $I_{pre} = 0$. Concerning Δ_2 in MC, the table reports a time range because this stage

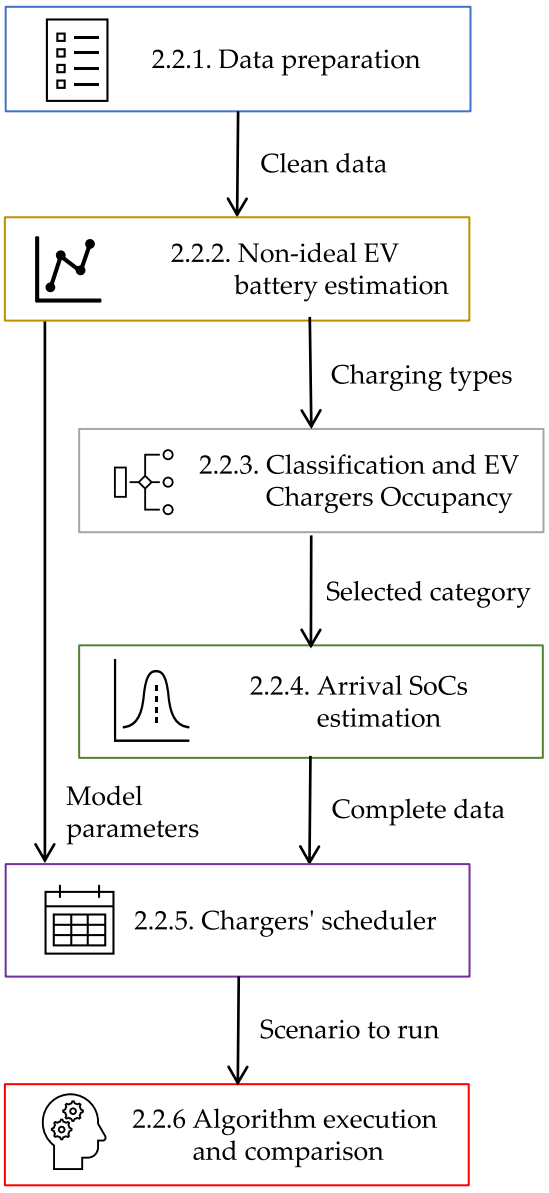

Fig. 2. General methodology followed by the EV CPO. The methodology is divided into six phases, each presented in different box colors and explained in the following subsections.

exhibits high variability depending on the arrival and departure SoCs of the EVs. Regarding the time Δ_3 in the CT stage, the table presents mean values of tails between 5 and 20 min (representing the majority of the data). However, as indicated in [37], the CT stage can have durations of around one hour. Moreover, different amounts of maximum powers and energies can be appreciated, from 2.5 kW to 6.9 kW, and from 10 kWh to 76 kWh, respectively. The power is computed with the 208 V of the EVSE reported by ACN [38]. Therefore, several EVs that charge at level 2 are identified and clustered into the three types.

2.2.3. Classification and EV chargers occupancy

In this phase, the three charging types undergo classification into several categories, facilitating the subsequent computation of EV charger occupancy for each category by assessing the arrival, departure, and duration time distributions (see to Fig. 6).

For the categorization of each charging type, the number of users for each type (refer to the Users quantity in Table 1) is weighted, resulting in nine categories encompassing all charging types. This includes five

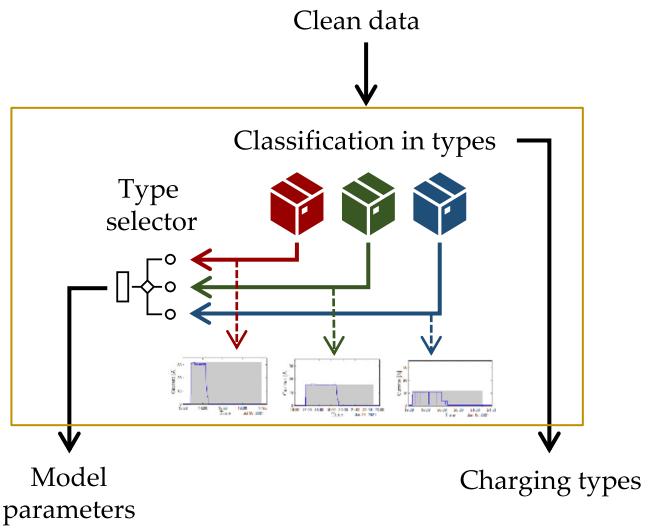

Fig. 3. Second phase of the methodology. Non-ideal EV battery estimation. Refer to the yellow box in the methodology presented in Fig. 2.

Table 1
Actual EV battery charging parameters.

Feature	Type 1	Type 2	Type 3
Users quantity [%]	67.1	30.6	2.3
Current I_{pre} [A]	7.7	8.3	8.6
Current I_{chg} [A]	31.7	16.4	10.6
Current I_{end} [A]	4.0	4.1	3.2
Time Δ_1 in PC	56”	49”	47”
Time Δ_2 in MC	[1’ – 15h53’]	[5’ – 9h26’]	[20’ – 1h16’]
Time Δ_3 in CT	11’	10’	0’
Max Energy [kWh]	75.5	36.5	9.7
Max Power [kW]	6.9	3.4	2.5

clusters for Type 1 (67.1% of users), three clusters for Type 2 (30.6% of users), and one cluster for Type 3 (2.3% of users). These nine categories are formulated by considering the maximum EV energy consumed by the EVs in each type. Table 2 illustrates the categories with distinct energy ranges for each type. Subsequently, the arrival and departure time distributions of each category are evaluated.

In Fig. 7, Fig. 8, and Fig. 9, the Probability Distribution Function (PDF) for each EV category is depicted. Each subset of figures corresponds to Type 1, Type 2, and Type 3. Notably, categories 2, 3, 4, 6, 7, 8, and 9 exhibit a distinct propensity for specific arrival times in the morning and departure times in the afternoon. Specifically, categories 2, 3, 4, 6, and 7 show EVs with a high probability of arriving between 8:00 and 10:00, and departing between 16:00 and 18:00. The occupancy duration periods for categories 2, 3, and 4 display two main tendencies, with the first being less than 1 h and the second around 7 h. Conversely, the occupancy duration for categories 6 and 7 is typically 1 and 8 h, respectively. Moreover, category 8 comprises EVs that prefer to arrive between 7:00 and 8:00, depart between 20:00 and 21:00, and consider two occupancy periods, the first lasting less than 1 h and the second around 12 h. In contrast, Category 9 involves EVs that favor arrival between 10:00 and 11:00, and departure between 19:00 and 20:00, with an occupancy period of around 12 h. Additionally, categories 1 and 5 encompass EVs with dual tendencies for both arrival and departure hours. Specifically, EVs from Category 1 generally arrive between 9:00 and 10:00 or between 13:00 and 17:00, and depart between 12:00 and 13:00 or between 16:00 and 17:00, with an occupancy period of around 1 h. Meanwhile, EVs from Category 5 typically arrive between 9:00 and 10:00 or between 18:00 and 19:00, depart between 18:00 and 19:00 or between 23:00 and 24:00, and have an occupancy period of around 1 or 6 h.

Table 2
Identified EVs per categories.

Type	Category	Quantity		Energy	Power	Battery
		Total [%]	Type [%]	[kWh]	[kW]	[kWh]
1	1	8.4	13.7	[0.7 – 8.9]	7.2	10.8
	2	29.2	42.1	[9.3 –26.4]	6.6	30.0
	3	16.6	24.1	[27.5 – 43.9]	7.4	50.0
	4	10.8	16.7	[45.0 – 58.9]	7.4	66.0
	5	2.1	3.4	[59.8 – 75.5]	7.4	86.4
2	6	23.2	76.5	[1.25 – 13.0]	3.7	14.9
	7	6.4	20.6	[13.5 – 17.7]	3.7	20.0
	8	1.0	2.9	[18.3 – 36.5]	3.6	40.0
3	9	2.3	100	[0.5 – 9.7]	2.8	10.8

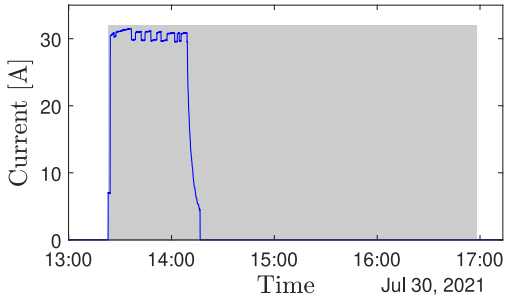

(a) Type 1.

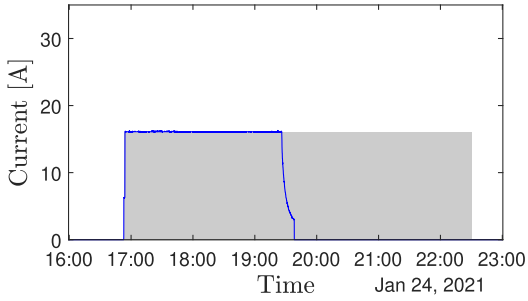

(b) Type 2.

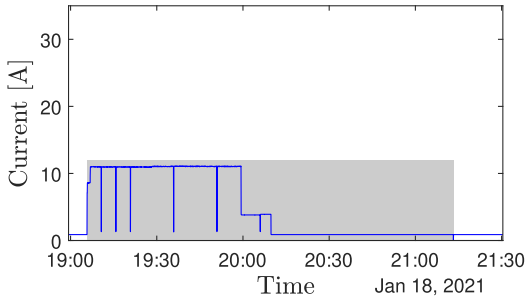

(c) Type 3.

Fig. 4. Examples of the identified EV batteries charging profiles per type. The gray areas denote the period when the EV is connected, while the blue profiles depict the actual EV current profiles with a maximum charging current of 32 A for Type 1, 16 A for Type 2, and 10 A for Type 3.

The substantial variations in arrival and departure times, as well as occupancy periods, significantly impact the effective power management of the chargers when operating in a coordinated strategy to achieve reliability.

2.2.4. EV arrival SoCs estimation

In this phase, distributions of the arrival SoC are estimated for each category based on the historical energy consumed by EVs. The EV arrival SoC is a critical variable when determining the amount of energy to inject into an EV. However, this variable is typically not reported, and calculating it is a challenging part of the Battery Management System (BMS) [39]. To estimate the arrival SoC of the EVs, we make assumptions about different EV battery capacities based on the historical energy consumed by each EV. We assume that the reported delivered energy is sufficient to achieve a fully charged battery, i.e., the EV departure SoC is always 100% (this information cannot be obtained from the database). Then, the arrival SoC of the EV_j can be estimated as:

$$\widetilde{SoC}_{j,a_j} = C_j - E_j, \tag{1}$$

where E_j is the delivered energy and C_j is the capacity of EV_j's battery. The capacity is calculated in Eq. (2), considering the maximum reported energy scaled by a factor γ. We assume that the historical maximum delivered energy from an EVSE to an EV corresponds to an arrival SoC between 10% and 20%. Therefore, γ is a factor between 1.1 and 1.2 to align with a typical commercial EV battery.

$$C_j = \gamma \; max\{E_j\} \tag{2}$$

Table 2 provides the nominal power and battery capacities of commercial EVs that align with the maximum power and energy of each category (refer to Table 1). This encompasses EVs with battery capacities ranging from 10.8 kWh to 86.4 kWh. The column labeled "Energy" outlines the range of energy delivered to the EVs in each category. It is noteworthy that the maximum energy falls between 80% and 90% of the commercial battery capacity reported in the last column.

By considering the commercial capacities from Table 2 and the energy data from the database, we can establish the distribution of the arrival SoC in each category. Fig. 10, Fig. 11, and Fig. 12 illustrates the arrival SoC distribution across the nine categories. Each subset of figures corresponds to Type 1, Type 2, and Type 3.

In particular, the distributions can be divided by SoC probability level as follows:

- *Low SoC*: Categories 1 and 7 exhibit a high probability of arriving with a low SoC between 10% and 20%. These SoCs, for instance, follow a Log-normal distribution.
- *Middle SoC*: EVs from categories 8 and 9 typically arrive with around 30% and 50% of the battery capacity. These SoCs, for example, follow a Weibull distribution.
- *High SoC*: In categories 3 and 4, the most probable arrival SoC is between 70% and 80%. These SoCs, for instance, follow a Beta distribution.
- *General SoC*: In categories 2, 5, and 6, a wide distribution is observed between 10% and 100%, with a higher probability in lower SoCs. Users in these categories lack a common pattern; they charge at any battery SoC. These SoCs, for example, follow a Chi-squared distribution.

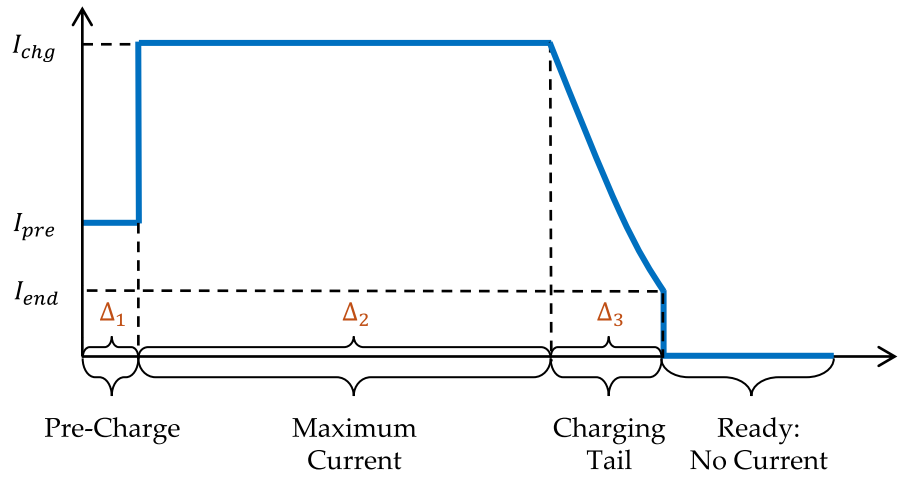

Fig. 5. Identified EV battery charging profile, considering three stages: PC, MC, and CT.

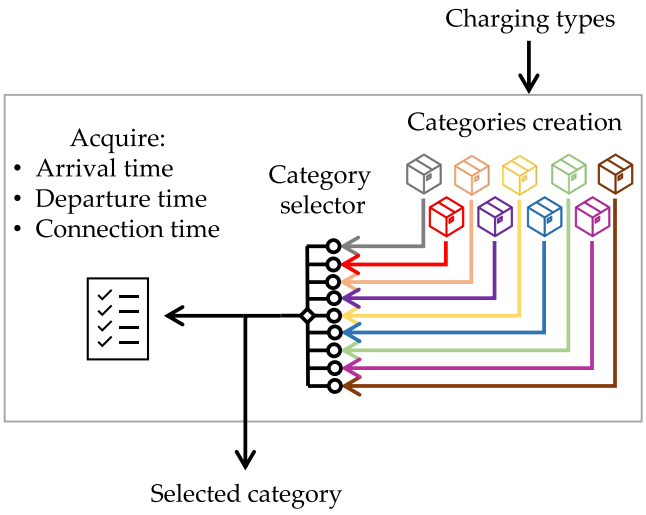

Fig. 6. Third phase of the methodology. Classification and EV Chargers Occupancy. Refer to the gray box in the methodology presented in Fig. 2.

Therefore, these arrival SoC distributions will provide crucial information for implementing smart EV algorithms and evaluating the flexibilities of different categories.

2.2.5. Chargers' scheduler

This phase aims to schedule the EVs in the workplace charging pool (see Fig. 13). Considering the comprehensive data from the preceding phases, the total number of charging events is allocated to the specific types or categories chosen. Subsequently, the individual charging events are randomly selected from the designated data, capturing the arrival and departure times, generating the arrival SoCs, and computing the battery capacities. Following this, the arrival and departure times are discretized into steps based on the simulation sample time, denoted as Δt. Finally, EVs are scheduled on the EV chargers, ensuring no overlap and maintaining at least one time slot between successive EV connection periods.

2.2.6. Algorithm execution and comparison

The final phase involves the execution of the algorithm, taking into account the schedule of EV chargers and energy prices (see Fig. 14). The optimal power profiles generated by the algorithm are then compared with the power profiles of the benchmark strategy. Various charging response metrics are subsequently computed, including the idle period.

The algorithm proposed is presented in the next section, along with the details of the benchmark strategy.

3. Smart EV charging strategy

In this section, we introduce the algorithm executed in the sixth and final phase of the methodology, as illustrated in Fig. 2. Smart charging (V1G) strategies outlined in the literature often neglect essential implementation features, such as the actual outputs of EVSE or the non-ideal battery responses. Furthermore, several standards for electrical connectors in EVs lack information regarding the SoC at the time of EV arrival. Neglecting these crucial features can lead to inaccuracies in coordination strategies, potentially causing issues in the electrical grid. To address these challenges, we propose a Model Predictive Control (MPC) algorithm designed to coordinate EV charging. This algorithm takes into account actual EVSE outputs, non-ideal battery responses, and the proposed EV arrival SoC distributions from the previous section.

3.1. Strategy features for charging EVs

The proposed MPC algorithm is designed to address the integration of EV chargers into the electrical grid, taking into account both the preferences of EV owners and the actual flexibility of the system. Concerning the actual EVSE output, the MPC algorithm considers the finite set of pilot signals outlined in the SAE J1772 standard. Specifically, the pilot signal can be either 0 A or a finite value ranging between 6 A and 32 A. The ACN-Data provides information on the EVSE pilot signal, revealing that the EV BMS generally charges at a lower current rate than the one set by the EVSE pilot. As a result, the algorithm restricts the EVSE's current to the actual delivered values reported in the data, assuming that the EV BMS will conform to the current imposed by the EVSE.

Furthermore, the algorithm models the EV battery as a non-ideal battery, considering the identified charging profiles presented in Fig. 4. It is crucial to note that the ideal battery response involves a constant power input from the arrival time until reaching full charge, essentially following only the Maximum Current (MC) stage (as depicted in Fig. 5). Given the absence of information from both the SAE J1772 standard and an EV app regarding the EV arrival SoC, the MPC algorithm utilizes the distributions proposed in the previous section (refer to Fig. 10, Fig. 11, and Fig. 12) as input for its operations.

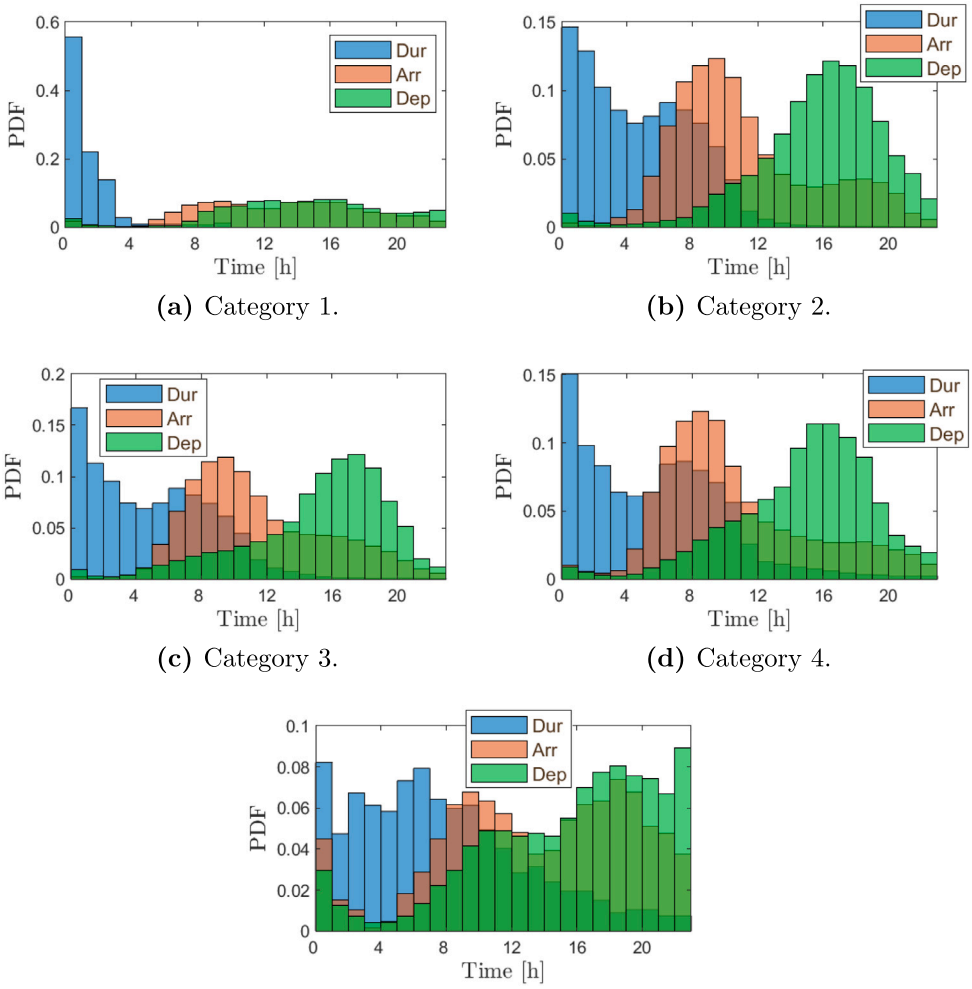

(a) Category 1. (b) Category 2.

(c) Category 3. (d) Category 4.

(e) Category 5.

Fig. 7. Distributions of arrival, departure, and duration in the identified EV categories for Type 1.

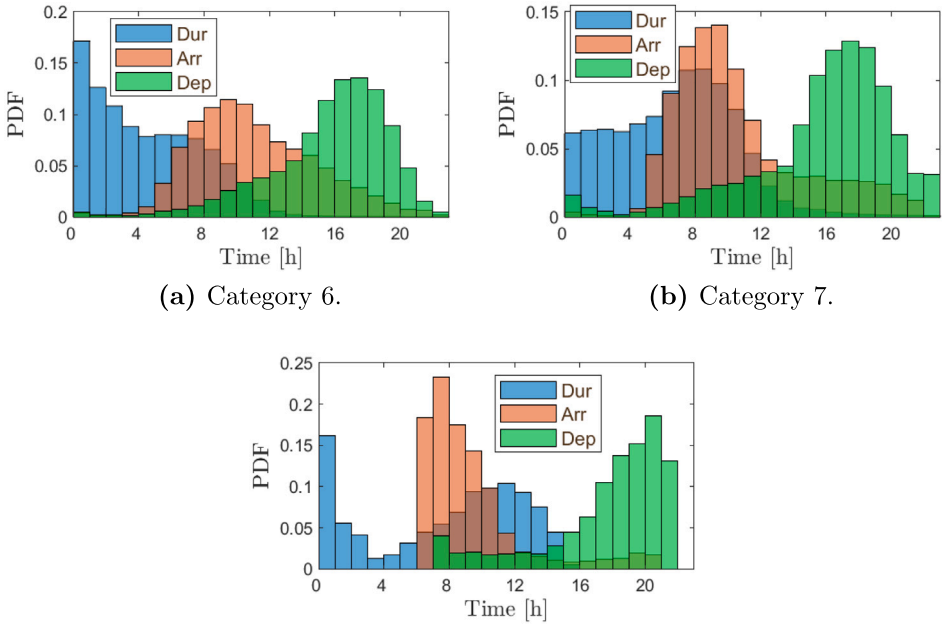

(a) Category 6. (b) Category 7.

(c) Category 8.

Fig. 8. Distributions of arrival, departure, and duration in the identified EV categories for Type 2.

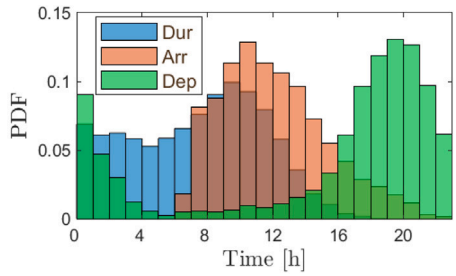

(a) Category 9.

Fig. 9. Distributions of arrival, departure, and duration in the identified EV category for Type 3.

3.2. EVSE model with non-ideal EV battery

The algorithm employs the charger model $x_{i,k}$ to predict the future output EV charger powers, where i represents the ith charger at the time slot k, as shown in Eq. (3). This model takes into account the dynamics of the single EVSE as presented in [33]. The model encompasses three possible conditions at step k based on the arrival a_j and departure d_j times of the jth EV, along with a binary variable $\xi_{i,k}$ indicating whether the ith charger has a plugged-in EV.

$$x_{i,k+1}=\begin{cases} \widetilde{SoC}_{j,a_j} & \text{if} \quad k=a_j \\ x_{i,k}+\Delta t P_{i,k} & \text{if} \quad a_j<k<d_j \\ 0 & \text{if} \quad \xi_{i,k}=0 \ \vee \ k=d_j \end{cases} \tag{3}$$

The first condition of the model relates to the estimated arrival SoC, denoted as $\widetilde{SoC}_{j,a_j}$. The second condition pertains to the evolution of the energy stored in the EV battery, assuming a duration Δt for the time slot k. The third condition is applied when there is no EV connected or when an EV is departing.

Typically, existing literature assumes that the EVSE nominal power represents the maximum power the EV battery can receive at any given moment, assuming ideal EV batteries. However, in this study, we propose an enhancement to the EVSE model that considers the non-ideal EV battery response observed in the data-driven characterization discussed in Section 2.2.2. As a result, we suggest limiting the EVSE power $P_{i,k}$ with a maximum power $P_{i,k,\max}$. It is important to note that this power is not constant but varies over time, following the battery charging profile illustrated in Fig. 5. In essence, the proposed constraint in Eq. (4) assumes that the EVSE voltage V remains constant

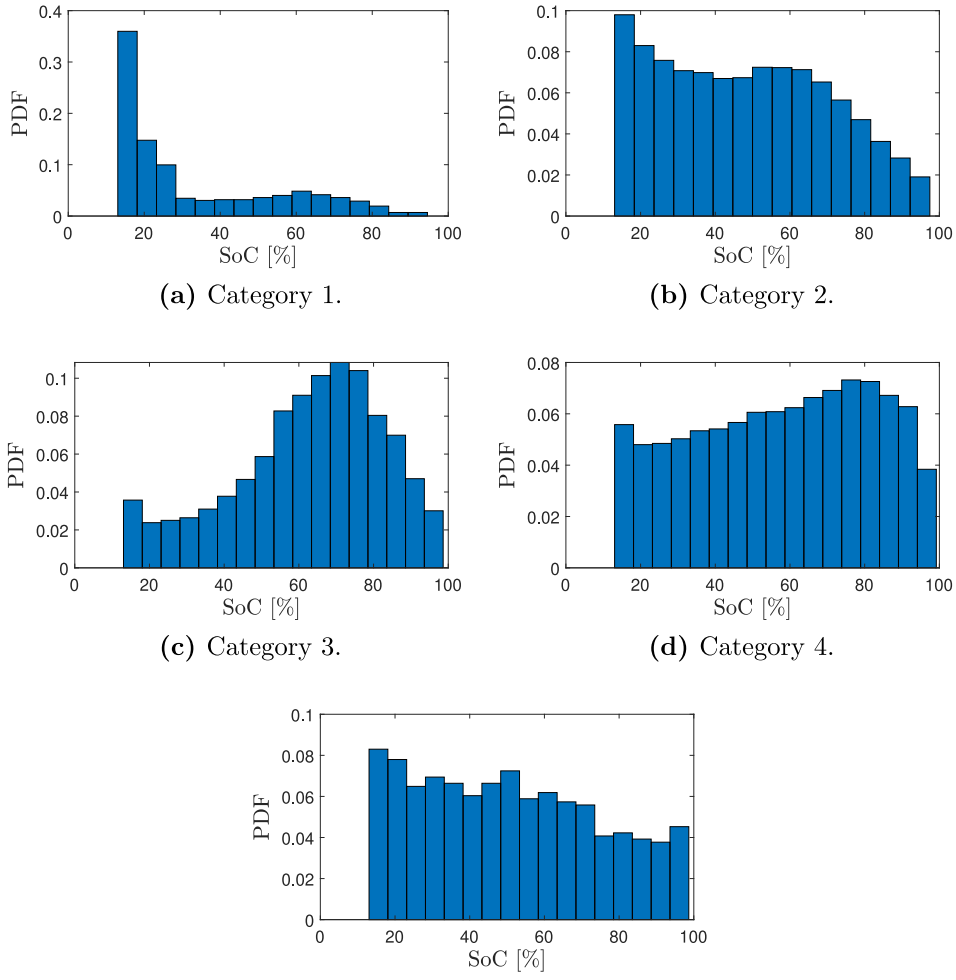

(a) Category 1. (b) Category 2.

(c) Category 3. (d) Category 4.

(e) Category 5.

Fig. 10. Arrival SoC distributions in the identified EV categories for Type 1.

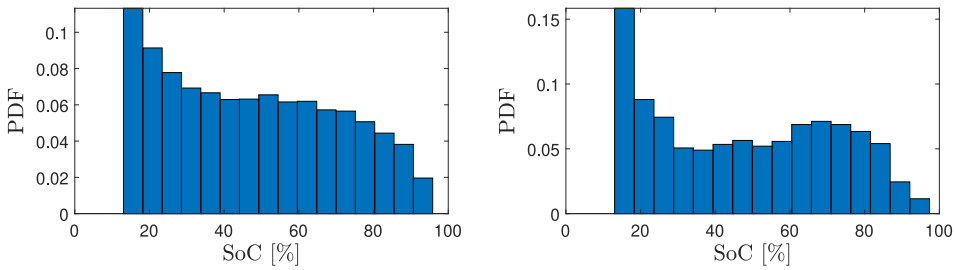

(a) Category 6. (b) Category 7.

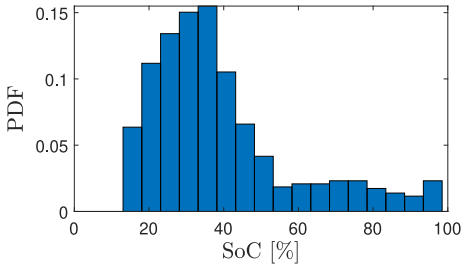

(c) Category 8.

Fig. 11. Arrival SoC distributions in the identified EV categories for Type 2.

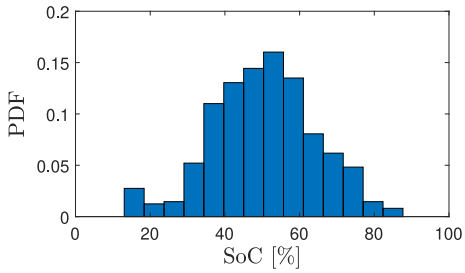

(a) Category 9.

Fig. 12. Arrival SoC distribution in the identified EV category for Type 3.

across all EV battery charging stages.

$$P_{i,k,\max}=\begin{cases} VI_{pre} & \text{if} \quad k \le \Delta_1 \\ VI_{chg} & \text{if} \quad k > \Delta_1 \wedge x_{i,k} \le x_{CT} \\ VI_{chg} - m x_{i,k} & \text{if} \quad x_{i,k} > x_{CT} \end{cases} \tag{4}$$

Moreover, drawing insights from [40], which indicates that the transition from the MC stage to the CT stage depends on the actual EV battery SoC, our constraint accommodates this by considering that the MC stage charges the batteries up to an SoC level x_{CT}, followed by a gradual current decrease with a slope m.

In any scenario, it is essential that the maximum power $P_{i,k,\max}$ remains within the bounds of the EVSE nominal output power $P_{i,\text{nom}}$, expressed as follows:

$$0 \le P_{i,k,\max} \le P_{i,\text{nom}}. \tag{5}$$

It is noteworthy that this enhancement to the non-ideal battery model applies to various EVSE dynamic models that assume ideal batteries. This is because the model itself remains unchanged, and only its maximum dispatchable power is adjusted.

3.3. Optimal control with minimum cost and maximum flexibility algorithm

This smart charging strategy proposes an enhancement to a charging coordinator previously introduced in Ref. [23]. We chose to improve this algorithm due to its potential benefits in flexibility capacity for the system operator, scalability, and granularity of decisions—providing optimal charging power for each charger at every time slot. In this study, we introduce an MPC algorithm that not only incorporates the improved EV battery model from the previous section but also accounts for the actual EVSE response and the maximum reduction in power demand. This reduction functions as an energy service and can be activated or deactivated.

The Optimal Control with Minimum Cost and Maximum Flexibility (OCCF) algorithm is formulated as an optimal control aiming to maximize charging flexibility while minimizing the operational cost of the EV CPO. The cost function is presented in Eq. (6), wherein two remuneration factors π^U and π^L are considered for upward ($U_{i,k}$) and downward ($L_{i,k}$) flexibilities.

$$\Delta t \sum_{k=0}^{H-1} \left(c_k \sum_{i=1}^{I} P_{i,k} - \pi^U \sum_{i=1}^{I} U_{i,k} - \pi^L \sum_{i=1}^{I} L_{i,k} \right) \tag{6}$$

Regarding the definition of the EVSE standard output, the power output is dependent on allowed discrete current levels, given by:

$$P_{i,k} = VI, \quad I \in \{0, 6, 7, \ldots, 32\}. \tag{7}$$

In this strategy, we ensure the minimum $\widetilde{SoC}j, d_j$ and maximum $\widehat{SoC}j, d_j$ state of charge at the departure time d_j as determined by the EV owner:

$$\widetilde{SoC}_{j,d_j} \le x_{i,d_j} \le \widehat{SoC}_{j,d_j} \tag{8}$$

The SoC capacity of the EV batteries is non-negative and relies on the individual EV battery's capacity. The nominal EV battery capacity is considered as the maximum capacity $x_{i,\max}$.

$$0 \le x_{i,k} \le x_{i,\max} \tag{9}$$

The EV charger power is constrained within the time slot k by the upward and downward flexibilities. Additionally, the power is restricted by the maximum power defined by the algorithm.

$$L_{i,k} \le P_{i,k} \le \xi_{i,k}(P_{i,k,\max} - U_{i,k}) \tag{10}$$

The flexibility bounds are defined as positive and not higher than the EVSE maximum power, as presented in Eq. (11).

$$0 \le U_{i,k} \le P_{i,\max} \quad \wedge \quad 0 \le L_{i,k} \le P_{i,\max} \tag{11}$$

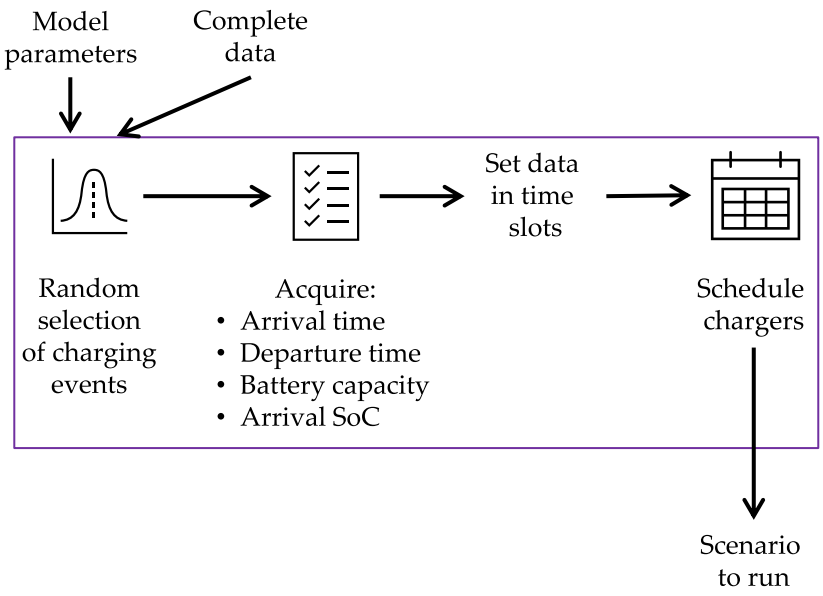

Fig. 13. Fifth phase of the methodology. Chargers' scheduler. Refer to the purple box in the methodology presented in Fig. 2.

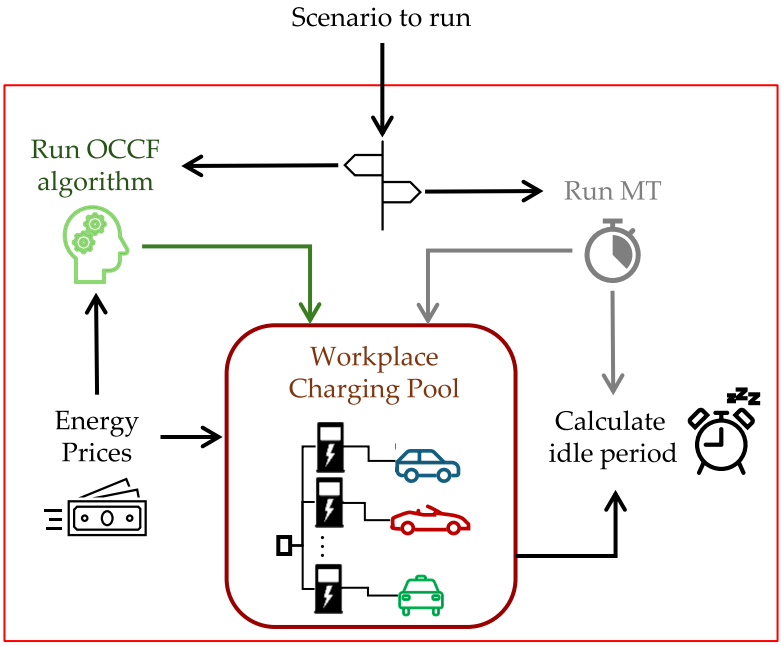

Fig. 14. Sixth phase of the methodology. Algorithm execution and comparison. Refer to the red box in the methodology presented in Fig. 2.

In addition, the constraint presented in Eq. (12) can be activated to provide Energy Services (ES), i.e., for reducing the power demanded in the EV charging pool.

$$\sum_{i=1}^{I} P_{i,k} \leq P_{T,\mathrm{ES}}, \quad \forall k \tag{12}$$

Notice that Eq. (12) acts as a limit for the power demand of the station at any time slot. Then, it can be activated for flexibility evaluation or for limiting the power station. In addition, the rebound effect can be avoided by limiting the power up to a period when the EV demand is low.

To summarize, the OCCF formulation considers the following constraints: the EVSE model presented in Eq. (3), the maximum variable power limit of Eq. (4), the EV charger output standard in Eq. (7), the minimum departure SoC decided by the owner in Eq. (8), the EV battery capacities in Eq. (9), the limits of the power in Eq. (10), and the upward and downward flexibility limits per EVSE in Eq. (11). The last constraint, i.e., Eq. (12), is activated only in case of providing an energy service.

The algorithm is executed for every time slot up to the total operation time β. At each slot, the algorithm runs for $k = 1, 2, \ldots, H$, considering $i = 1, 2, \ldots, I$ chargers, and $j = 1, 2, \ldots, J$ EVs (J is not always the same; it depends on the vehicles connected at every time slot). H is the MPC prediction horizon.

The complexity of the problem followed in the paper is greater than in [23], in which the algorithm deals with a Linear Programming (LP) problem. In fact, our improved algorithm follows a Mixed-Integer Nonlinear Programming (MINLP) problem that has as decision variables the optimal profiles $P_{i,k}$; the $U_{i,k}$ and $L_{i,k}$ flexibilities of the ith charger; and the maximum power limit $P_{i,k,\max}$. Notice that $P_{i,k}$ depends on a set of discrete values of I (see Eq. (7)), while $P_{i,k,\max}$ depends on three possible state (see Eq. (4)). Besides, the maximum power reduction

$P_{T,\mathrm{ES}}$ is calculated in an iterative optimization, maximizing its value and achieving a feasible solution.

The complexity of the problem can be summarized as follows:

- The size of the state and decisions variables, $x_{i,k}$, $P_{i,k}$, $U_{i,k}$, $L_{i,k}$, and $P_{i,k,\max}$ respectively, is $I \cdot H$.
- The number of constraints in $x_{i,k}$ is $3 \cdot I \cdot H$, for each time slot; $\cdot I \cdot H$ allocated for the lower and the upper bounds, and the other for the charger dynamics.
- The number of constraints in $P_{i,k}$ is $3 \cdot I \cdot H$, for each time slot, $I \cdot H$ for the lower bounds, $I \cdot H$ for the upper bounds, and $I \cdot H$ for the integer power outputs.
- The number of constraints in $P_{i,k,\max}$ is $3 \cdot I \cdot H$, for each time slot, $I \cdot H$ for the lower bounds, $I \cdot H$ for the upper bounds, and $I \cdot H$ for the power that depends on the EV battery charging period.
- The number of constraints in $U_{i,k}$ and $L_{i,k}$ is $2 \cdot I \cdot H$ per each one, for each time slot, half for the lower bounds, and a half for the upper bounds.
- The number of constraints in the minimum SoC requirement $\widetilde{SoC}_{j,d_j}$ depends on the number of EV connected.

The problem's complexity increases linearly with H, indicating that an expansion in the number of chargers would result in a proportional increase in the number of constraints and decision variables.

Contrary to the approach in Ref. [23], the CVX package is inadequate for solving this problem because of the nonlinearities introduced by the piecewise functions in Eq. (4). Consequently, alternative solvers are essential, and in this study, the Gurobi solver is employed.

3.4. Minimum time

In this strategy, power is treated as a continuous variable, defined as:

This subsection presents an uncoordinated charging strategy that looks for charging the EVs in the charging pool with the maximum allowed power $P_{i,k,max}$ until the EV reaches its full capacity $SoC_{i,max}$ or earlier if the EV is desired to be disconnected. In this strategy, power is treated as a continuous variable, defined as:

$$P_{i,k,\max} = V I_{chg} \tag{13}$$

This guarantees the Minimum Time (MT) for the charging event, where the delivered power abruptly transitions from maximum power to zero when there is no EV connected or when the EV is fully charged. Notice that this strategy does not consider the time-varying energy price, nor the possibility of adjusting its energy consumption.

3.5. Idle period for flexibility

The flexibility of EV power capacity is contingent on the idle time of the EV. Consequently, this idle time is calculated as the time difference between the parking time and the charging completion time in the uncoordinated (MT strategy). The idle period of the jth EV, expressed as a percentage, is defined as:

$$t_{j,idle} = \frac{d_{j,done} - a_j}{d_j - a_j} 100, \tag{14}$$

where $d_{j,done}$ is the time when the EV is charged. Notice that $d_{j,done}$ and d_j are not necessarily at the same time.

4. Simulation results

In this section, we introduce various case studies involving EV chargers in workplace scenarios. We begin by outlining the implementation details of the case studies. Subsequently, we conduct a comprehensive analysis, ranging from single charger responses to an overall assessment of the charging pool managed by the CPO. The assessment of the charging pool is accomplished through multiple simulation campaigns, exploring the responses of different EV types and categories. The simulations demonstrate the effectiveness of the EV charging algorithm by presenting results related to maximum power reduction and cost savings for workplace EV chargers.

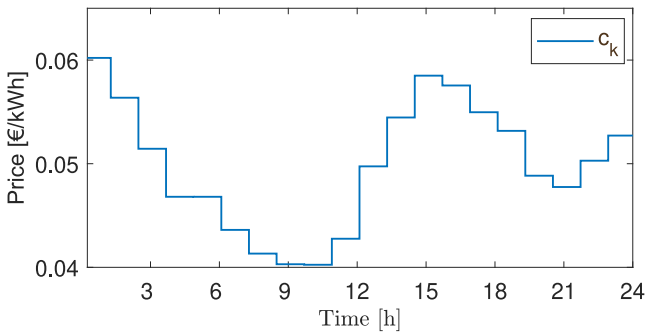

Fig. 15. Hourly electrical energy price sequence.

4.1. Implementation of the case studies

The simulations adhere to the methodology outlined in the flow diagram illustrated in Fig. 2. Charging events are specifically selected, focusing on those with parking periods ranging from 30 min to 12 h, collectively representing 95% of all charging events. The average daily count of charging events is computed at 67, with individual EVSEs accommodating between 1 and 3 charging events daily. Notably, a single charger can host a maximum of 7 charging events in a day.

Within the charger scheduler, the total number of charging events is categorized into the selected types or categories. Subsequently, specific charging events are randomly chosen from this dataset, incorporating arrival and departure times, generating arrival SoCs, and calculating battery capacities. These times are then discretized into steps based on the simulation sample time, denoted as Δt. Following this, EVs are scheduled at the EV chargers. Finally, the proposed OCCF algorithm is executed, taking into account the EV chargers' schedule and the energy prices. The power profiles generated by the OCCF algorithm are then compared with those derived from the MT strategy.

The sequence of electrical energy prices is sourced from the Entso-e Transparency Platform [41]. By analyzing one year of data, the mean prices per hour are computed. This mean price, depicted in Fig. 15, is uniformly applied across all case studies.

A crucial parameter to configure is the CT stage of the EV battery charging profile (refer to Fig. 5). As previously assessed, the CT stage commences after reaching a specific SoC level in the EV battery. However, not all EVs have the same SoC level at this switching point. For instance, Ref. [42] establishes that the SoC for switching to the CT stage in a lithium-ion battery is close to 85%. Furthermore, in [43], lithium-ion batteries are considered, indicating that the switching SoC depends on the EV battery technology. Therefore, for the case studies, switching SoC x_{CT} is defined as a random variable with a uniform distribution between 85% and 100%.

4.2. Single EVSE evaluation

The initial simulation campaign is designed to showcase the effectiveness of the strategy by evaluating the response of a single EVSE. The simulation considers all types of data. To assess the enhanced OCCF algorithm's performance, the strategy's results are compared not only with the benchmark MT strategy but also with the OCCF strategy introduced in [23], denoted as OCCF_{Ideal} in this study. The EV CPO operation time is presented between 6:00 and 24:00 h.

The response of the single EVSE is depicted in Fig. 16. This EVSE charges four EVs during the evaluated period. Specifically, Fig. 16(a)

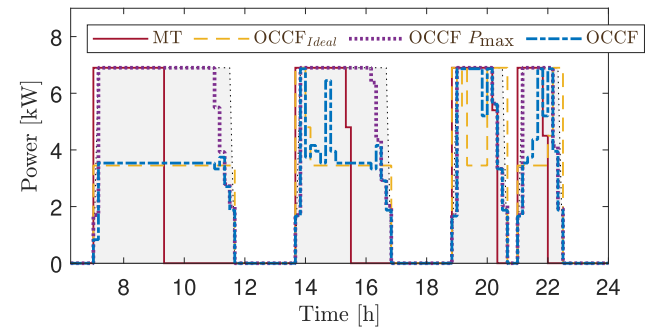

(a) Power.

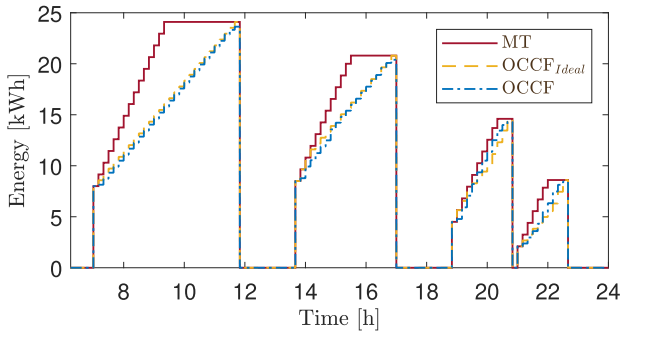

(b) Energy.

Fig. 16. Power demand and energy consumption for each strategy at a single charger.

illustrates the power profiles defined by each strategy. The MT strategy's response is represented in red, demonstrating how the strategy charges the EVs with a constant maximum power from the arrival time a_j to the full charge time $d_{j,done}$. The original OCCF strategy, OCCF$_{Ideal}$, is presented in yellow, showcasing different levels of power. Due to lower prices, the third and fourth EVs charge with maximum power near the departure time. However, this presents an issue because these EV batteries might not charge up to the desired departure SoC due to the actual battery performance allowing lower power near 100% SoC.

Additionally, the figure presents the decision variables of the proposed enhanced OCCF algorithm: the maximum power $P_{i,k,\max}$ in purple and the output power $P_{i,k}$ in blue. Concerning the maximum power, it is evident how the identified EV battery charging profile is generated with the PC, MC, and CT stages. Furthermore, the EVSE output power shows how this algorithm aims to inject power during low-energy price periods while charging the EVs with a medium power value, allowing the provision of upward and downward flexibility if requested. Notably, this proposed strategy considers the non-ideal battery response, resulting in lower power injection near 100% SoC. The jumps in power align with the discrete current values defined in Eq. (7).

On the other hand, Fig. 16(b) depicts the energy evolution in the EVs (up to 100% charge). The figure intentionally omits to display the percentage of SoC to enable the reader to observe the diverse EV battery capacities. Notably, the MT strategy reaches the departure SoC first. In contrast, both OCCF algorithms achieve the departure SoC nearly at the departure time, gaining an advantage to enhance the flexibility of the EVSE.

4.3. Charging pool analysis

In this subsection, an evaluation of the power demanded by the charging pool is performed. The simulation implementation considers all types of data, and the parameters employed in the simulation are detailed in Table 3.

Table 3
EV charging pool simulation parameters.

Name	Symbol	Value	Notes
EV charging pool sample time	Δt	10 min	–
Operation time of the station	β	24 h	144 iterations
Prediction horizon	H	12 h	72 iterations
Battery capacity in EV$_j$	C_j	{10.8 – 86.4}	–
Nominal EVSE output power	$P_{i,\text{nom}}$	7.4 kW	Level 2
Minimum SoC in EV$_j$ at departure	$\overline{SoC}_{j,d_j}$	100%	$x_{i,d_j} = C_j$
Remuneration price	π^U , π^L	c_k	–
Number of EVSEs	I	55	–
Number of EVs	J	67	–

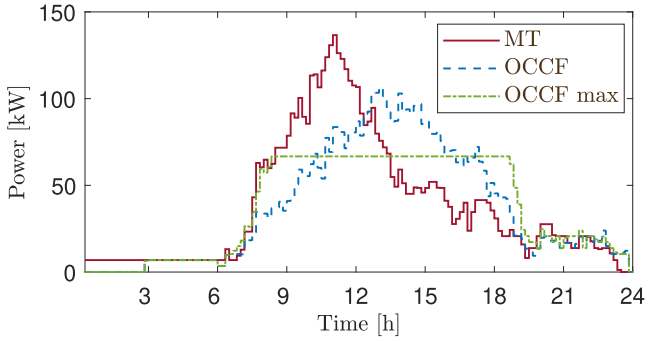

Fig. 17. Power demanded by the chargers considering all EV types.

The results are evaluated not only for both strategies, OCCF and MT, but also for the OCCF with maximum power reduction, denoted as OCCF max. In this case study, the maximum power reduction $P_{T,\text{ES}}$ that can be requested as an ES, is assumed as the maximum reduction from the peak power of the uncoordinated strategy $P_{T,\text{un,max}}$ in an operation period. Note that this power limit is a parameter in Eq. (12), and these simulations aim to demonstrate the potential for reducing peak power. Then, the power is computed as:

$$P_{T,\text{ES}} = P_{T,\text{un,max}} - \sum_{i=1}^{I} P_{i,k}. \tag{15}$$

Fig. 17 presents the results of the strategies. It is important to note that the delivered energy is the same between the strategies but in different time slots, enabling peak reduction for safe grid operation and a reduction in the operation costs of the CPO that manages the charging pool. Furthermore, the power reduction achieved by OCCF max is especially beneficial for distribution grids with connected commercial loads, as described in [44]. These loads typically maintain high and constant power demand between 8:00 and 19:00. Therefore, implementing this strategy to control workplace chargers can effectively mitigate morning peak power.

Table 4 presents the key results of this simulation in the column named General, showcasing a significant peak reduction of 22.0% achieved by implementing the OCCF strategy. However, the OCCF max strategy demonstrates an even more substantial peak reduction, reaching up to 51.2%—effectively cutting the peak demand in half and mitigating risks to the electrical grid. It is noteworthy that this effective power management relies on the judicious utilization of EVSE flexibility, which is influenced by the idle time of EVs. The workplace chargers exhibit an average idle period of 43%.

Moreover, the OCCF max strategy exhibits no rebound effect due to its constrained limit, ensuring normal operation after providing the service, facilitated by the occupancy distribution in workplace chargers (see Fig. 7, Fig. 8, and Fig. 9).

Concerning operational costs, there is a marginal reduction of about 2.8% and 1.3%. However, it is important to note that we have not considered the revenues generated from flexibility availability or the

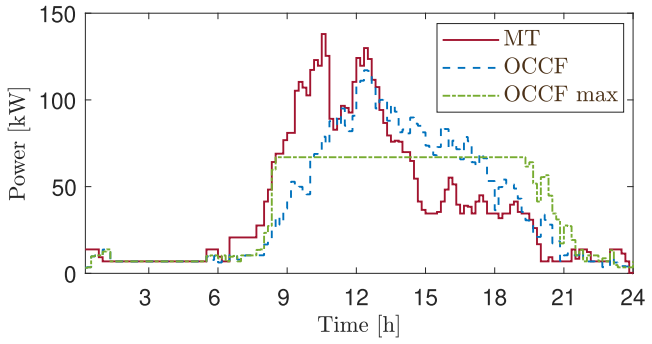

(a) Type 1.

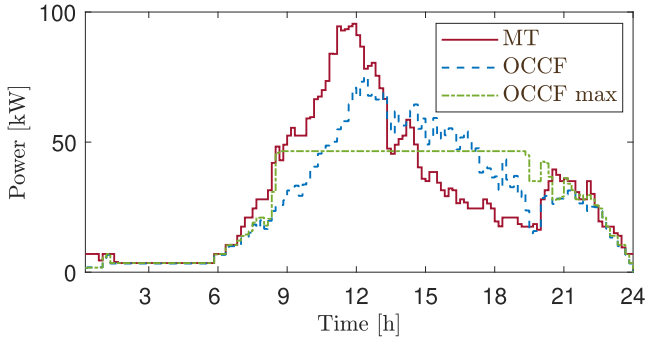

(b) Type 2.

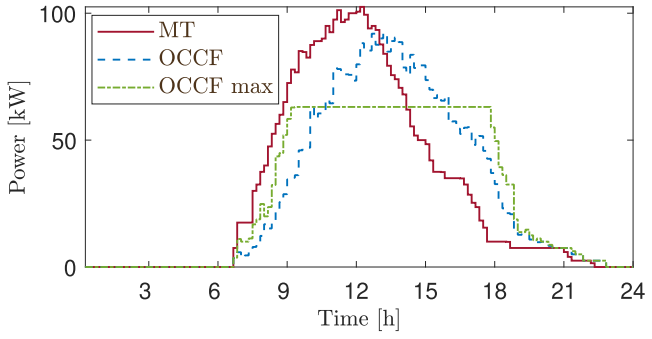

(c) Type 3.

Fig. 18. Power demanded by the chargers per type.

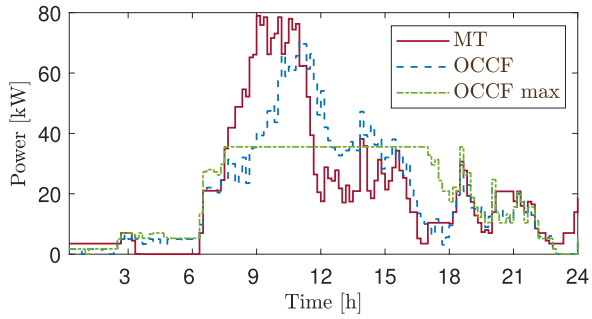

(a) *Low SoC*: Categories 1, 7

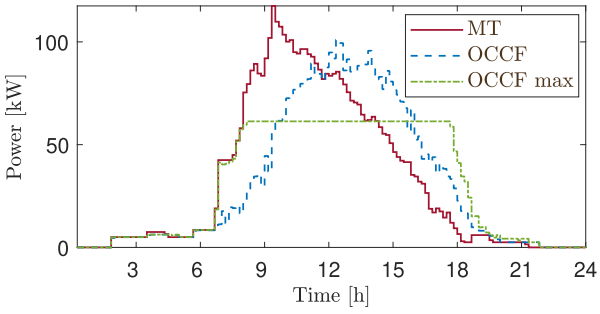

(b) *Middle SoC*: Categories 8, 9

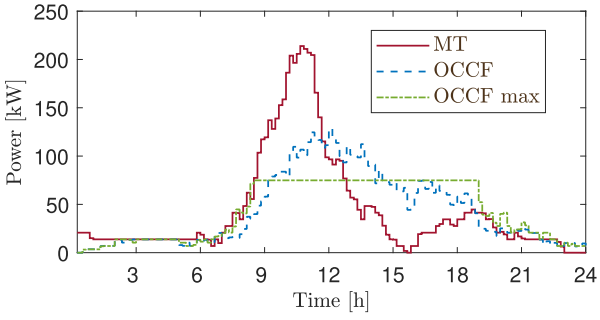

(c) *High SoC*: Categories 3, 4

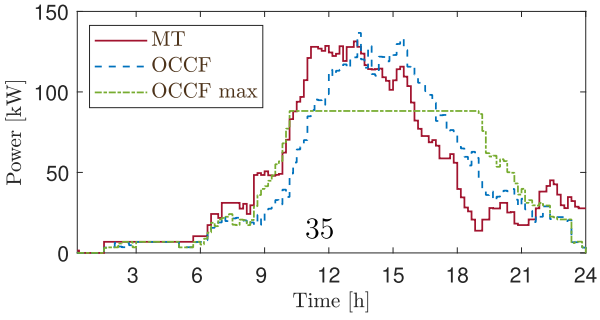

(d) *General SoC*: Categories 2, 5, 6

Fig. 19. Power demanded by the chargers per set of arrival SoC.

income derived from providing energy services. Therefore, the OCCF algorithm not only avoids increasing operational costs but also enables the station to participate in energy services, resulting in significant income generation.

4.4. Types evaluation

In this subsection, we assess the three identified EV types. Three simulations are conducted: the first considering only EVs from Type 1, the second only Type 2, and the third only Type 3. As in the previous simulation, the implementation is carried out following the parameters reported in Table 3.

The results are depicted in Fig. 18 and reported in Table 4. It can be observed that the delivered energy is higher in Type 1, while in Type 3, it is lower. This is an expected result due to the power level delivered to each type.

The average idle period for Type 1 is almost half of the time the EVs are connected. Typically, EV users parking in workplace chargers have similar occupancy periods; thus, in Type 1, the injected power is higher than in the others, charging Type 1 EVs first in the MT strategy and allowing a longer idle time. Notice that this type has the majority of EV users, which helps increase flexibility and reduce the peak power in the OCCF max strategy by 51.5% compared to the MT strategy.

The OCCF algorithm is effective in reducing the CPO operation cost, which depends on energy price variations. However, the algorithm attempts to inject power at every time slot to maximize its ability

Table 4
Smart charging response performance.

Feature	General	Types			Arrival SoC probability			
		1	2	3	Low	Middle	High	General
Delivered Energy [kWh]	902.0	937.9	731.4	702.9	507.7	762.2	1,046.4	1,158.9
Average idle period [%]	43.6	48.7	31.9	33.9	35.5	38.4	42.8	37.5
Peak power in MT [kW]	136.6	138.0	95.5	102.5	79.0	117.5	213.9	131.4
Peak power in OCCF [kW]	106.5	117.1	75.3	92.1	70.7	101.1	128.5	136.7
Peak power in OCCF max [kW]	66.7	67.0	46.5	63.1	35.6	61.3	74.9	88.2
OCCF power reduction [%]	22.0	15.1	21.2	10.1	10.5	14.0	39.9	−4.0
OCCF max power reduction [%]	51.2	51.5	51.3	38.5	55.0	47.8	65.0	32.9
Cost in MT [€/kWh]	290.9	300.6	235.4	225.5	166.6	243.9	338.7	366.8
Cost in OCCF [€/kWh]	282.8	293.8	221.8	218.5	160.1	232.9	329.4	356.7
Cost in OCCF max [€/kWh]	287.2	299.7	225.2	221.9	160.0	236.7	332,4	363.3
Charging savings in OCCF [%]	2.8	2.3	5.8	3.1	3.9	4.5	2.8	2.8
Charging savings in OCCF max [%]	1.3	0.3	4.3	1.6	3.9	3.0	1.9	0.9

to provide energy services across most time slots. Consequently, the station can charge EVs during periods of high energy prices, generating income from energy services during these periods.

It is noteworthy that the peak power in Type 3 is higher than in Type 2, which is unexpected given the injected power at each type. However, this is due to the parking hours in Type 3 having less variance, leading to a concentration of charging events around midday, whereas Type 2 has more evenly distributed parking hours, resulting in a more distributed energy consumption throughout the day.

4.5. Categories assessment

In this subsection, the study focuses on different EV categories. Four simulations are conducted, considering the category sets outlined in Section 2.2.4, which account for arrivals with low SoC, middle SoC, high SoC, and general SoC. As in the previous simulation, the parameters used are detailed in Table 3.

The results are presented in Fig. 19 and summarized in Table 4. The low arrival SoC set, encompassing categories 1 and 7, comprises EVs with small batteries that require minimal energy capacities, representing a large SoC for these EVs. This suggests that some of these users likely own hybrid plug-in EVs. Consequently, the energy delivered in this set is small, irrespective of whether the EVs arrive with a low SoC. In contrast, the high SoC set features EVs with large batteries that demand high energy capacities, indicating lower initial SoCs. This may imply that these users are more conservative, aiming to maintain a higher battery SoC.

Concerning the idle period, the high SoC set exhibits the most extended idle period at 42.8%, resulting in a substantial power reduction of 65% in the OCCF max strategy. This implies that EVs in this set require minimal time for charging in the MT strategy, allowing the OCCF algorithm to leverage high flexibility. Conversely, the low SoC set shows the shortest idle period, as these EVs spend most of their time charging their batteries.

The OCCF power reductions align with expectations: higher arrival SoC corresponds to greater power reduction due to increased flexible charging time. However, the OCCF max power reductions do not follow the same pattern. In the middle SoC set, the peak power reduction is lower than in the low SoC set, which is unexpected. This is attributed to high EV penetration occurring for a brief period in the morning when users in the low SoC set arrive at work. Consequently, the charger's output power can be shifted. In contrast, the middle SoC set experiences more evenly distributed EV penetration over an extended period.

5. Conclusion

A sophisticated Electric Vehicle (EV) charging pool algorithm managed by a workplace Charger Point Operator (CPO) has been proposed. This algorithm adeptly handles the non-ideal responses of EV batteries and adheres to the EV charger pilot signal standard. Developed through a model predictive control framework, the algorithm seeks to minimize EV CPO costs while maximizing the charger's flexibility. The model formulation is enhanced by constraining the maximum power of the EV charger based on the identified EV battery response, leading to improved and precise dispatch powers.

To better understand workplace chargers' behavior, a categorization strategy based on data-driven approaches is introduced. Nine categories are established, considering user energy consumption and three identified power levels. A methodology for estimating EV battery arrival state of charge distributions is defined. These categories are then grouped based on the arrival state of charge, impacting the flexibility each group offers to the system.

Several simulation campaigns validate the effectiveness of the EV charging algorithm. Comparative analyses with a typical minimum time strategy show notable reductions in peak power, with up to 51.2% reduction in a typical scenario and 65% in scenarios where EVs arrive with a high state of charge. Importantly, these power reductions exhibit no rebound effect. Cost reductions, ranging from 0.3% to 5.8%, are observed in the evaluated scenarios. However, this article does not consider remuneration payments for the flexibility services, which would further increase the CPO's income.

This innovative tool facilitates the integration of EV charging pools into the electrical grid without compromising CPO operations and ensures economic benefits. Future work will focus on assessing the remuneration calculation for the flexibility provided by the optimal algorithm. Additionally, adjustments will be made to enable vehicle-to-grid operations.

CRediT authorship contribution statement

Cesar Diaz-Londono: Writing – review & editing, Writing – original draft, Software, Methodology, Investigation, Formal analysis, Data curation, Conceptualization. **Gabriele Fambri:** Writing – review & editing, Software, Methodology, Data curation, Conceptualization. **Paolo Maffezzoni:** Writing – review & editing, Supervision, Conceptualization. **Giambattista Gruosso:** Writing – review & editing, Writing – original draft, Validation, Supervision, Resources, Methodology, Investigation, Formal analysis, Data curation, Conceptualization.

Declaration of competing interest

The authors declare that they have no known competing financial interests or personal relationships that could have appeared to influence the work reported in this paper.

Data availability

Data will be made available on request.

Acknowledgment

This research was funded by FSE-REACT EU, PON "RICERCA e INNOVAZIONE" 2014–2020, Azione IV.6 (Green).

References

[1] Global EV outlook 2022. Report, IEA; 2022.
[2] Das H, Rahman M, Li S, Tan C. Electric vehicles standards, charging infrastructure, and impact on grid integration: A technological review. Renew Sustain Energy Rev 2020;120:109618. http://dx.doi.org/10.1016/j.rser.2019.109618.
[3] Calearo L, Marinelli M, Ziras C. A review of data sources for electric vehicle integration studies. Renew Sustain Energy Rev 2021;151:111518. http://dx.doi.org/10.1016/j.rser.2021.111518.
[4] Wulff N, Miorelli F, Gils HC, Jochem P. Vehicle energy consumption in Python (VencoPy): Presenting and demonstrating an open-source tool to calculate electric vehicle charging flexibility. Energies 2021;14(14). http://dx.doi.org/10.3390/en14144349.
[5] Gonzalez Venegas F, Petit M, Perez Y. Plug-in behavior of electric vehicles users: Insights from a large-scale trial and impacts for grid integration studies. eTransportation 2021;10:100131. http://dx.doi.org/10.1016/j.etran.2021.100131.
[6] Dudek E. The flexibility of domestic electric vehicle charging: The electric nation project. IEEE Power Energy Mag 2021;19(4):16–27. http://dx.doi.org/10.1109/MPE.2021.3072714.
[7] Unterluggauer T, Rauma K, Järventausta P, Rehtanz C. Short-term load forecasting at electric vehicle charging sites using a multivariate multi-step long short-term memory: A case study from Finland. IET Electr Syst Transp 2021;11(4):405–19. http://dx.doi.org/10.1049/els2.12028.
[8] Janjic A, Velimirovic L, Stankovic M, Petrusic A. Commercial electric vehicle fleet scheduling for secondary frequency control. Electr Power Syst Res 2017;147:31–41. http://dx.doi.org/10.1016/j.epsr.2017.02.019.
[9] Lee JH, Chakraborty D, Hardman SJ, Tal G. Exploring electric vehicle charging patterns: Mixed usage of charging infrastructure. Transp Res D 2020;79:102249. http://dx.doi.org/10.1016/j.trd.2020.102249.
[10] Helmus JR, Lees MH, van den Hoed R. A data driven typology of electric vehicle user types and charging sessions. Transp Res C 2020;115:102637. http://dx.doi.org/10.1016/j.trc.2020.102637.
[11] Al-Dahabreh N, Sayed MA, Sarieddine K, Elhattab M, Khabbaz MJ, Atallah RF, et al. A data-driven framework for improving public EV charging infrastructure: Modeling and forecasting. IEEE Trans Intell Transp Syst 2023;1–14. http://dx.doi.org/10.1109/TITS.2023.3337324.
[12] Zhao Y, Jiang Z, Chen X, Liu P, Peng T, Shu Z. Toward environmental sustainability: data-driven analysis of energy use patterns and load profiles for urban electric vehicle fleets. Energy 2023;285:129465. http://dx.doi.org/10.1016/j.energy.2023.129465.
[13] Nimalsiri NI, Mediwaththe CP, Ratnam EL, Shaw M, Smith DB, Halgamuge SK. A survey of algorithms for distributed charging control of electric vehicles in smart grid. IEEE Trans Intell Transp Syst 2020;21(11):4497–515. http://dx.doi.org/10.1109/TITS.2019.2943620.
[14] Tan B, Chen H, Zheng X, Huang J. Two-stage robust optimization dispatch for multiple microgrids with electric vehicle loads based on a novel data-driven uncertainty set. Int J Electr Power Energy Syst 2022;134:107359. http://dx.doi.org/10.1016/j.ijepes.2021.107359.
[15] Giordano F, Arrigo F, Diaz-Londono C, Spertino F, Ruiz F. Forecast-based V2G aggregation model for day-ahead and real-time operations. In: 2020 IEEE power and energy society innovative smart grid technologies conference. 2020, p. 1–5. http://dx.doi.org/10.1109/ISGT45199.2020.9087659.
[16] Diaz-Londono C, Vuelvas J, Gruosso G, Correa-Florez CA. Remuneration sensitivity analysis in prosumer and aggregator strategies by controlling electric vehicle chargers. Energies 2022;15(19). http://dx.doi.org/10.3390/en15196913.
[17] Gruosso G, Ruiz FO. Electric vehicle fleets as balancing instrument in micro-grids. Energies 2021;14(22). http://dx.doi.org/10.3390/en14227616.
[18] Yao E, Liu T, Lu T, Yang Y. Optimization of electric vehicle scheduling with multiple vehicle types in public transport. Sustainable Cities Soc 2020;52:101862. http://dx.doi.org/10.1016/j.scs.2019.101862.
[19] Lakshminarayanan V, Chemudupati VGS, Pramanick SK, Rajashekara K. Real-time optimal energy management controller for electric vehicle integration in workplace microgrid. IEEE Trans Transp Electr 2019;5(1):174–85. http://dx.doi.org/10.1109/TTE.2018.2869469.
[20] Wang M, Mu Y, Shi Q, Jia H, Li F. Electric vehicle aggregator modeling and control for frequency regulation considering progressive state recovery. IEEE Trans Smart Grid 2020;11(5):4176–89. http://dx.doi.org/10.1109/TSG.2020.2981843.
[21] Zhang J, Sun K, Li C, Yang H, Zhou B, Hou X, et al. MPC-based co-optimization of an integrated PV-eV-Hydrogen station to reduce network loss and meet EV charging demand. eTransportation 2023;15:100209. http://dx.doi.org/10.1016/j.etran.2022.100209.
[22] Hussain A, Bui V-H, Musilek P. Local demand management of charging stations using vehicle-to-vehicle service: A welfare maximization-based soft actor-critic model. eTransportation 2023;18:100280. http://dx.doi.org/10.1016/j.etran.2023.100280.
[23] Diaz-Londono C, Colangelo L, Ruiz F, Patino D, Novara C, Chicco G. Optimal strategy to exploit the flexibility of an electric vehicle charging station. Energies 2019;12(20). http://dx.doi.org/10.3390/en12203834.
[24] Sadeghianpourhamami N, Refa N, Strobbe M, Develder C. Quantitive analysis of electric vehicle flexibility: A data-driven approach. Int J Electr Power Energy Syst 2018;95:451–62. http://dx.doi.org/10.1016/j.ijepes.2017.09.007.
[25] Gerritsma MK, AlSkaif TA, Fidder HA, van Sark WGJHM. Flexibility of electric vehicle demand: Analysis of measured charging data and simulation for the future. World Electr Veh J 2019;10(1). http://dx.doi.org/10.3390/wevj10010014.
[26] Diaz-Londono C, Maffezzoni P, Daniel L, Gruosso G. Flexibility of electric vehicle chargers in residential, workplace, and public locations based on real-world data. In: IEEE EUROCOn 2023 - 20th international conference on smart technologies. 2023, p. 354–9. http://dx.doi.org/10.1109/EUROCON56442.2023.10199090.
[27] Gschwendtner C, Knoeri C, Stephan A. The impact of plug-in behavior on the spatial–temporal flexibility of electric vehicle charging load. Sustainable Cities Soc 2023;88:104263. http://dx.doi.org/10.1016/j.scs.2022.104263.
[28] Sevdari K, Calearo L, Andersen PB, Marinelli M. Ancillary services and electric vehicles: An overview from charging clusters and chargers technology perspectives. Renew Sustain Energy Rev 2022;167:112666. http://dx.doi.org/10.1016/j.rser.2022.112666.
[29] Giraldo JS, Bañol Arias N, Salazar Duque EM, Hoogsteen G, Hurink JL. A compensation mechanism for EV flexibility services using discrete utility functions. In: 2022 IEEE PES innovative smart grid technologies conference Europe. 2022, p. 1–6. http://dx.doi.org/10.1109/ISGT-Europe54678.2022.9960542.
[30] Frendo O, Graf J, Gaertner N, Stuckenschmidt H. Data-driven smart charging for heterogeneous electric vehicle fleets. Energy AI 2020;1:100007. http://dx.doi.org/10.1016/j.egyai.2020.100007.
[31] Xu J, Guo Z, Xu Z, Zhou X, Mei X. A systematic review and comparison of liquid-based cooling system for lithium-ion batteries. eTransportation 2023;17:100242. http://dx.doi.org/10.1016/j.etran.2023.100242.
[32] Yao E, Wong VWS, Schober R. Robust frequency regulation capacity scheduling algorithm for electric vehicles. IEEE Trans Smart Grid 2017;8(2):984–97. http://dx.doi.org/10.1109/TSG.2016.2530660.
[33] Diaz C, Ruiz F, Patino D. Smart charge of an electric vehicles station: A model predictive control approach. In: 2018 IEEE conference on control technology and applications. 2018, p. 54–9. http://dx.doi.org/10.1109/CCTA.2018.8511498.
[34] Gupta V, Konda SR, Kumar R, Panigrahi BK. Multiaggregator collaborative electric vehicle charge scheduling under variable energy purchase and EV cancelation events. IEEE Trans Ind Inf 2018;14(7):2894–902. http://dx.doi.org/10.1109/TII.2017.2778762.
[35] SAE electric vehicle and plug in hybrid electric vehicle conductive charge coupler J1772 201710. Standard, SAE International; 2017.
[36] Lee ZJ, Li T, Low SH. ACN-data: Analysis and applications of an open EV charging dataset. In: Proceedings of the tenth ACM international conference on future energy systems. 2019, p. 139–49. http://dx.doi.org/10.1145/3307772.3328313.
[37] Sun C, Li T, Low SH, Li VO. Classification of electric vehicle charging time series with selective clustering. Electr Power Syst Res 2020;189:106695.
[38] Lee ZJ, Lee G, Lee T, Jin C, Lee R, Low Z, et al. Adaptive charging networks: A framework for smart electric vehicle charging. IEEE Trans Smart Grid 2021;12(5):4339–50. http://dx.doi.org/10.1109/TSG.2021.3074437.
[39] Zhang M, Fan X. Review on the state of charge estimation methods for electric vehicle battery. World Electr Veh J 2020;11(1). http://dx.doi.org/10.3390/wevj11010023.
[40] Peng W. Accurate circuit model for predicting the performance of lead-acid AGM batteries [Master's thesis], University of Nevada at Las Vegas; 2011.
[41] ENTSO-E Transparency Platform. 2022, https://transparency.entsoe.eu/. [Accessed 10 October 2022].
[42] Battery University BU-409: Charging Lithium-ion. 2021, https://batteryuniversity.com/article/bu-409-charging-lithium-ion. [Accessed 10 January 2022].
[43] Qian K, Zhou C, Allan M, Yuan Y. Modeling of load demand due to EV battery charging in distribution systems. IEEE Trans Power Syst 2011;26(2):802–10. http://dx.doi.org/10.1109/TPWRS.2010.2057456.
[44] Jardini J, Tahan C, Gouvea M, Ahn S, Figueiredo F. Daily load profiles for residential, commercial and industrial low voltage consumers. IEEE Trans Power Deliv 2000;15(1):375–80. http://dx.doi.org/10.1109/61.847276.